remote sensing

MDPI

Article

An Empirical Model to Estimate Abundance of Nanophase Metallic Iron ($npFe^0$) in Lunar Soils

Dawei Liu [1,*], Yuanzhi Zhang [1,2], Guangliang Zhang [1], Bin Liu [1], Xin Ren [1], Rui Xu [3] and Chunlai Li [1]

[1] Key Laboratory of Lunar and Deep Space Exploration, National Astronomical Observatories, Chinese Academy of Sciences, Beijing 100101, China; zhangyz@nao.cas.cn (Y.Z.); zhanggl@nao.cas.cn (G.Z.); liub@nao.cas.cn (B.L.); renx@nao.cas.cn (X.R.); licl@nao.cas.cn (C.L.)

[2] School of Astronomy and Space Science, University of Chinese Academy of Sciences, Beijing 100049, China

[3] Key Laboratory of Space Active Opto-Electronics Technology, Shanghai Institute of Technical Physics, Chinese Academy of Sciences, Shanghai 200083, China; xurui@sitp.ac.cn

* Correspondence: liudw@nao.cas.cn

Received: 23 February 2020; Accepted: 19 March 2020; Published: 24 March 2020

Abstract: Lunar soils gradually become mature when they are exposed to a space environment, and nanophase metallic iron ($npFe^0$) generates within them. $npFe^0$ significantly changes the optical properties of lunar soils and affects the interpretation of the remotely sensed data of the lunar surface. In this study, a correlation analysis was conducted between $npFe^0$ abundance and reflectance spectra at short wavelengths for lunar soil samples in four size groups based on their spectral and compositional data, collected by the Lunar Soil Characterization Consortium (LSCC). Results show that 540 nm single scattering albedo (SSA) of lunar soils correlates well with their corresponding $npFe^0$ abundance for each size group of lunar soil samples. However, it is poorly correlated with $npFe^0$ abundance when all size groups were considered because of the strong interference from grain size variation of lunar soils. To minimize the effect of grain size, the correlation of $npFe^0$ abundance with the spectral ratio of 540 nm/810 nm SSA of all size groups for LSCC samples was calculated and results show that a higher correlation existed between them ($R^2 = 0.91$). This ratio can serve as a simple empirical model for estimating $npFe^0$ abundance in lunar soils. However, bias could be introduced to the estimation result when lunar soils possess a high content of agglutinitic glass and ilmenite. Our future work will focus on improving the model's performance for these lunar soils.

Keywords: $npFe^0$; single scattering albedo; lunar soil characterization consortium

1. Introduction

Space weathering represents any natural processes pursuing an airless planetary body that largely modify its surface material's physical and compositional characteristics [1,2]. It is mainly induced by solar wind ion implantation and micrometeoroid bombardment and has been generally applied to planetary observations, such as on the Moon or Mercury as well as asteroids [3–6]. Space weathering also influences the reflectance spectra of planetary surface materials and reduces our capability to remotely evaluate the planetary mineralogy and composition on their surface [1,7].

Samples from the Moon and asteroids provide us an opportunity to research space weathering of an airless body. Actually, when the Apollo soil samples were brought back to the Earth-based laboratories, the measured results of lunar soils quickly showed that their reflectance is very different from that of pulverized lunar rocks [7–9]. In comparison with the optical properties of pulverized lunar rocks, the spectral reflectance of lunar soils shows a red-sloped continuum (namely reddening), a lower albedo (namely darkening), and attenuated absorption bands [1,10]. Early literature attributed

these optical changes to the presence of dark amorphous "glass" or "agglutinate" in lunar soils [11]. However, subsequent laboratory and remote sensing measurement have showed that these optical properties of lunar soils are caused by the accumulation of fine grained nanophase metallic iron ($npFe^0$) residing in amorphous rims of lunar soil grains after a long duration exposure of fresh lunar soils to a space weathering environment [12–16]. Two major mechanisms have been proposed to explain the accumulation of $npFe^0$ within lunar soils. One is solar wind ion implantation stating that surface material of lunar soil grains such as O atoms are preferentially sputtered from their lattice sites as a result of ion-irradiation, generating a reducing environment in which iron particles within residue surface material are reduced to form $npFe^0$ [10,17–19]. The other mechanism proposed that because of continuous impact of micrometeoroids, lunar soil grains are vaporized so that some FeO molecules are dissociated into their constituent neutral atoms [10,20]. The O atoms dissipate, and the iron atoms deposit and accumulate on the surface of lunar soil grains as $npFe^0$ [21]. A number of laboratory experiments have been carried out to simulate the process of solar wind bombardment and micrometeorite impact events to investigate space weathering and the formation of $npFe^0$ [21–28]. For example, Duke et al. [22] irradiated an olivine sample with 1.0 keV H^+ and 4 keV He^+ to simulate solar wind implantation and found that the surface of iron of olivine is dramatically reduced to the metallic form. The process of micrometeorite impacts was simulated by [25,26] using pulse-laser irradiation on the olivine and pyroxene grains. Results show that lunar-like $npFe^0$ could form within the amorphous rims of mineral grains and the darkening and reddening effect on the spectra of these grains can be observed after pulse-laser irradiation. By performing slow- and rapid-heating experiments on mature lunar soils, Thompson et al. [21] simulated micrometeorite impact events and provided the first direct in-situ observation of $npFe^0$ formation within lunar soil grains. In addition to the generation of $npFe^0$, recent work also suggests that nanoparticles of Fe^{2+} and Fe^{3+} oxidation states could also form within sub-mature and mature lunar soils as a result of space weathering [29].

Estimation of $npFe^0$ abundance in lunar soils is a very interesting topic for many lunar scientists. It is helpful to accurately evaluate the lunar surface's mineralogy and composition using remotely sensed measurement. Currently, Hapke's radiative transfer model (RTM) has been generally applied to assess the mineralogy of the lunar surface owing to its ability to account for the effects of space weathering. Estimation of $npFe^0$ abundance in lunar soils is a necessary critical input for accurate Hapke's RTM mineral abundance inversion. The $npFe^0$ has been also associated with the presence of H_2O/OH^- due to reduction of Fe^{2+} to $npFe^0$ by impinging solar wind with the release of H_2O/OH^- in lunar soils [30]. This brings about a highly possible usage of $npFe^0$ to determine lunar surface regions with H_2O/OH^- [31]. In addition, determination of the abundance of $npFe^0$ in lunar soils helps us to understand the formation of lunar swirls, which were once attributed to deficient $npFe^0$ as a result of retarded space weathering [32–34].

Despite the significant importance of $npFe^0$, its abundance in lunar soils has not been widely quantitatively evaluated [35–38]. Some previous studies attempted to establish models that can relate the measured reflectance spectra of lunar soils to their characteristic ferromagnetic resonance (I_s) induced by $npFe^0$. I_s is highly linearly correlated with the abundance of $npFe^0$ and can be used as a measure of $npFe^0$ in lunar soils [39–41]. According to the measured reflectance spectra and I_s of 35 lunar soil samples, Hiroi et al. [35] found that I_s shows a good linear correlation with the spectral slope defined by a straight-line tangent to the shoulders of a 1 μm absorption band of lunar soils. Mouélic et al. [36] expanded the number of investigated lunar samples to 50 and found that I_s can be also evaluated by the continuum slope derived from the ratio of 1500 nm/750 nm reflectance. Pieters et al. [37] developed several statistically optimized formulations that can link I_s of lunar soils with their corresponding Clementine-bands-based spectral parameter according to the compositional and spectral data acquired by the Lunar Soil Characterization Consortium (LSCC). Compared with the work of [35,36], more samples of lunar soil were used in their investigation and the sample dataset shows a larger variation in composition and maturity which is well suited for characterizing the spectral properties of lunar soils. Recent work estimating the abundance of $npFe^0$ in lunar soils has

been done by Trang and Lucey [38], who derived the $npFe^0$ abundance by using Hapke's RTM and constraining the input FeO and ilmenite content of lunar soils.

While these previous studies have provided possible ways to predict $npFe^0$ or I_s of lunar soils, the practical use of these methods will be impeded by several limitations. For example, most of these works require band information at longer wavelength (e.g., 1500 nm) to define the spectral slope [35,36], which is difficult in some cases. On the one hand, the spectral range of many remote sensing sensors stops at around 1 μm and no longer-wavelength data are available (e.g., Clementine, Chang'E-1 Interference Imaging Spectrometer). On the other hand, it is a challenge to accurately define a continuum slope when lunar soils become highly mature or lack apparent absorption features at around 1 μm [35]. In addition, the model for $npFe^0$ estimation could be too complex to be applied. Many input parameters and pre-knowledge on the compositional information of lunar soils are required before the model can be used, which is difficult to obtain in advance [38].

Here, we developed a simple empirical model to estimate $npFe^0$ abundance in lunar soils from measured reflectance data. This model correlates the $npFe^0$ abundance with the ratio of single scattering albedo (SSA) of two wavelengths outside the absorption bands of lunar soils and requires no longer-wavelength spectral data. Grain size effects of lunar soils on $npFe^0$ abundance estimation are partially removed according to this model.

2. Dataset

The dataset of the Lunar Soil Characterization Consortium (LSCC) [7,15] was applied in the study to develop the model. The dataset includes 10 highland and 9 mare soil samples. Each soil sample was grouped into four types of grain sizes (< 10 μm, 10–20 μm, 20–45 μm, and < 45 μm). The maturity index (I_s/FeO), composition (e.g. FeO content) and reflectance spectra of each size group (altogether 76 data samples) were measured by the LSCC (Table 1). The spectral data of these soil samples can be downloaded from Reflectance Experiment Laboratory (Relab) of Brown University (http://www.planetary.brown.edu/relabdocs/LSCCsoil.html). The maturity index, composition and mineralogy information of corresponding soil samples can be acquired from the Planetary Geoscience Institute of the University of Tennessee (https://pgi.utk.edu/lunar-soil-characterization-consortium-lscc-data/). Correlation was analyzed for all the samples except for sample 71061 in that it is abundant in black beads [42], with very different optical properties from those of other samples [15,43].

Table 1. Lunar Soil Characterization Consortium (LSCC) dataset used in this study.

Sample	FeO (%)	I_s/FeO	Ilmenite (%)	Agglutinitic Glass (%)	Grain Size	Highland/Mare
10084	12	145	5	62.6	<10 μm	Mare
12001	12.5	115	1.6	61.9	<10 μm	Mare
12030	14.3	32	3	55	<10 μm	Mare
15041	11	161	0.7	70.4	<10 μm	Mare
15071	9.59	159	1.2	59.7	<10 μm	Mare
70181	12.7	104	3.4	58.3	<10 μm	Mare
71501	13.5	88	7.6	53.1	<10 μm	Mare
79221	11.3	169	5.2	61.5	<10 μm	Mare
14141	7.66	14.5	1.7	45.9	<10 μm	Highland
14163	8.83	87	1.1	66.3	<10 μm	Highland
14259	7.82	174.8	1.5	71.6	<10 μm	Highland
14260	8.1	144.9	1.3	66.5	<10 μm	Highland
61141	3.66	119.3	0.3	61.6	<10 μm	Highland
61221	3.64	19.8	0.9	41.6	<10 μm	Highland
62231	3.63	169	0.4	69.5	<10 μm	Highland
64801	3.84	115.2	0.2	63.6	<10 μm	Highland
67461	3.35	35.2	0.2	35.8	<10 μm	Highland

Table 1. *Cont.*

Sample	FeO (%)	I_s/FeO	Ilmenite (%)	Agglutinitic Glass (%)	Grain Size	Highland/Mare
67481	3.61	38.5	0.2	35.2	<10 μm	Highland
10084	14.7	87	5.2	57	10–20 μm	Mare
12001	15.9	67	1.8	56.8	10–20 μm	Mare
12030	17.2	17	3.2	49.8	10–20 μm	Mare
15041	14.4	92	0.8	56.7	10–20 μm	Mare
15071	15.4	80	1.8	49.2	10–20 μm	Mare
70181	15.5	63	6.7	51.7	10–20 μm	Mare
71501	16.4	50	9.7	44.8	10–20 μm	Mare
79221	15	78	6	54.3	10–20 μm	Mare
14141	9.46	11.6	1.1	48.6	10–20 μm	Highland
14163	10.1	64.8	0.9	58.5	10–20 μm	Highland
14259	9.71	101.8	1.2	68.7	10–20 μm	Highland
14260	9.84	98.9	1	65.2	10–20 μm	Highland
61141	5.14	81.6	0.3	53.9	10–20 μm	Highland
61221	4.4	13.89	0.3	32.6	10–20 μm	Highland
62231	4.86	109.9	0.5	55	10–20 μm	Highland
64801	4.78	84.9	0.2	61	10–20 μm	Highland
67461	4.64	23.9	0.3	32.4	10–20 μm	Highland
67481	4.04	33	0.2	28.6	10–20 μm	Highland
10084	15.5	67	6.4	53.9	20–45 μm	Mare
12001	16.9	51	2.6	56.2	20–45 μm	Mare
12030	17.6	12	2.6	39.4	20–45 μm	Mare
15041	15.2	66	1.2	51.3	20–45 μm	Mare
15071	15.6	49	1.9	47.6	20–45 μm	Mare
70181	16	53	8.9	43.4	20–45 μm	Mare
71501	17.8	28	12.3	38.3	20–45 μm	Mare
79221	15.8	57	7.3	46.5	20–45 μm	Mare
14141	11.6	5.8	1.9	41	20–45 μm	Highland
14163	11.5	43.2	0.8	56.4	20–45 μm	Highland
14259	11	77.2	1.3	60.5	20–45 μm	Highland
14260	10.7	80.2	0.9	64	20-45 μm	Highland
61141	5.15	75.5	0.3	50.1	20–45 μm	Highland
61221	4.62	8.4	0.6	28.9	20–45 μm	Highland
62231	5.31	80.7	0.3	50.6	20–45 μm	Highland
64801	4.82	83.4	0.3	53.6	20–45 μm	Highland
67461	4.93	22.3	0.3	25.4	20–45 μm	Highland
67481	5.19	20.7	0.1	27.6	20–45 μm	Highland
10084	14.8	88			<45 μm	Mare
12001	16	62			<45 μm	Mare
12030	16	20			<45 μm	Mare
15041	14.2	93			<45 μm	Mare
15071	14.9	71			<45 μm	Mare
70181	15.3	61			<45 μm	Mare
71501	16.5	44			<45 μm	Mare
79221	14	91			<45 μm	Mare
14141	9.81	9.7			<45 μm	Highland
14163	9.94	66.5			<45 μm	Highland
14259	9.54	108.6			<45 μm	Highland
14260	9.65	93.3			<45 μm	Highland
61141	4.8	94.5			<45 μm	Highland
61221	4.47	13.6			<45 μm	Highland
62231	4.87	116.7			<45 μm	Highland
64801	4.68	92.2			<45 μm	Highland
67461	4.24	29.8			<45 μm	Highland
67481	4.38	33.5			<45 μm	Highland

Note: agglutinitic glass and ilmenite contents for size group < 45 μm are not provided in LSCC dataset

3. Method

3.1. Strong Influence of npFe^0 at Short Wavelengths

Liu et al. and Liu. [44,45] conducted sensitivity analyses of a suite of Hapke's RTM-simulated reflectance spectra of lunar soils with the aim of quantitatively determining the relative importance of npFe^0 abundance, grain size and mineral abundance in controlling the optical properties of lunar soils. Results show that npFe^0 has strong influences in the full spectral ranges as compared to mineral abundance. The simulated spectral reflectance of lunar soils is more sensitive to the variation of npFe^0 at shorter spectral regions than longer spectral ranges. The strong npFe^0 effect on short-wave bands is evident in the spectral reflectance of LSCC data, which tend to be convergent in short spectral regions for different sizes of grains in each sample of lunar soils (Figure 1). This indicates that the spectral reflectance of lunar soils in short wavelengths is less sensitive to the variation of composing minerals of lunar soils, while mainly controlled by the variation of npFe^0 abundance [44,45]. The strong influence of npFe^0 at short wavelengths can be also demonstrated by the work of [46], who prepared a suite of analog soils of varying abundance of npFe^0 to study the optical effects of npFe^0 on the measured reflectance spectra. Result shows that npFe^0 (<10 nm) greatly reddens short wavelengths spectra while leaving the longer wavelengths spectra mostly unaffected. Using lunar samples of similar composition but distinct exposure age, Fischer et al. and Fischer and Pieters [47,48] attempted to develop a mathematical model that can describe the optical alteration of lunar soils due to space weathering. Their work suggests that the effect of npFe^0 on the optical properties of lunar soils can be evaluated as a function of wavelength with an increasing rate of darkening toward short wavelengths. This result is also consistent with Mie theory, which states that if the npFe^0 is smaller than the wavelength of incident light, the greatest amount of light extinction will be at the short wavelengths region [48]. Combing Hapke's RTM and Mie theory to model the scattering behavior of npFe^0, Wohlfarth et al. [49] also found a strong influence of npFe^0 at short wavelengths of simulated reflectance spectra.

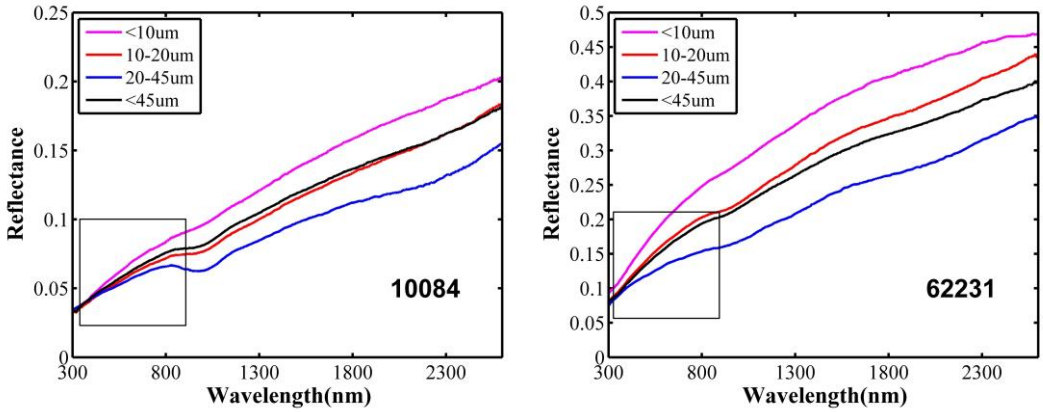

Figure 1. Reflectance spectra of four grain size groups of lunar soil samples 10084 and 62231. Black squares show the convergence of reflectance spectra at short wavelengths.

3.2. Estimation of npFe^0 Abundance in Lunar Soils

The strong effect of npFe^0 on short wavelengths spectra motivates us to explore the correlation between the npFe^0 abundance of lunar soils and their spectral of corresponding reflectance values only at short spectral ranges. Through conducting ferromagnetic resonance measurement on lunar soil samples, Morris [41] found a linear relation among npFe^0 abundance, FeO content and maturity index (I_s/FeO), reproduced below:

$$\text{npFe}^0 = \left(3.2 \times 10^{-4}\right)(\text{FeO})(I_s/\text{FeO}) \quad (1)$$

In this study, the abundance of npFe^0 for each lunar sample was first obtained via Equation (1) based on the measured maturity index (I_s/FeO) and FeO content (Table 1). Then, the LSCC measured

spectral reflectance of each sample was re-sampled to the same bands as Moon Mineralogy Mapper (M^3) data and transformed to single scattering albedo (SSA) using a simplified Hapke's RTM (Appendix A and Equation (A2) of [50]). This transformation has potential to remove the effects of multiple scattering because $npFe^0$ residing in the rims of soil grains mainly influences SSA of lunar soils. Considering the influence of $npFe^0$ increases with decreasing wavelength [44,45], 540 nm SSA, which is the first available band of M^3 data of high quality, was chosen for the correlation analysis with the obtained $npFe^0$ abundance. Finally, the correlation of $npFe^0$ abundance with the spectral ratio of 540 nm SSA/810 nm SSA was also calculated, aiming at minimizing the effect of grain size of lunar soils on $npFe^0$ estimation. The band at 810 nm was selected because it is outside the absorption wavelength regions of lunar soils, and the influence of composing minerals on $npFe^0$ estimation could be minimized.

4. Result

4.1. Correlation between 540 nm Single Scattering albedo (SSA) and $npFe^0$

Figure 2 shows the correlation of $npFe^0$ abundance with 540 nm SSA of all samples of LSCC soils. In general, as the abundance of $npFe^0$ increases, the SSA of the corresponding lunar soil decreases, which is consistent with the darkening effect of $npFe^0$, as expected. However, for all groups of investigated soil samples, the $npFe^0$ does not show a good correlation with the corresponding SSA at 540 nm. This could be attributed to the influence of grain size variation of lunar soils at short wavelengths. In addition to the varying abundance of $npFe^0$, the grain size of lunar soils is also a significant factor driving the measured reflectance. For example, the spectral reflectance of a suite of transparent materials with different sizes of grains was measured by Adams and Filice [51] and Pieters [52], whereby it was noted that there is a general increase in the overall reflected spectra with decreasing grain size.

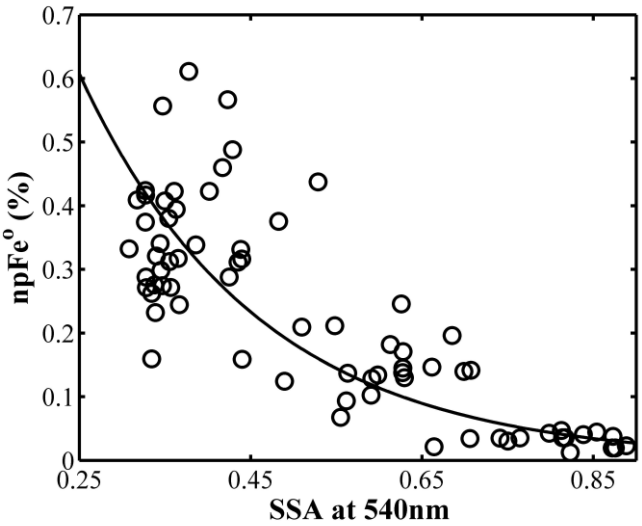

Figure 2. Correlation of SSA at 540 nm with $npFe^0$ for all size groups of LSCC soils.

To validate this speculation, correlation was analyzed for each group of sizes of LSCC samples seen in Figure 3. It is clear that the $npFe^0$ of each size group highly correlates to the SSA at 540 nm, with the determination (R^2) close to or higher than 0.90 (Table 2). The abundance of $npFe^0$ in each size group of LSCC data can be well fitted in the form of an exponential function as $Y = \alpha e^{(-\beta X)}$. Here, X is SSA at 540 nm, Y is the abundance of $npFe^0$, and α and β are two regressed constants. Detailed values of α, β and R^2 for each size group samples are referred to Table 2. The regression lines for 10–20 μm and the < 45 μm size groups have similar α and β (Table 2) because the reflectance spectra of bulk soil (< 45 μm) are most similar to that of a 10–20 μm size fraction [1] (Figure 1).

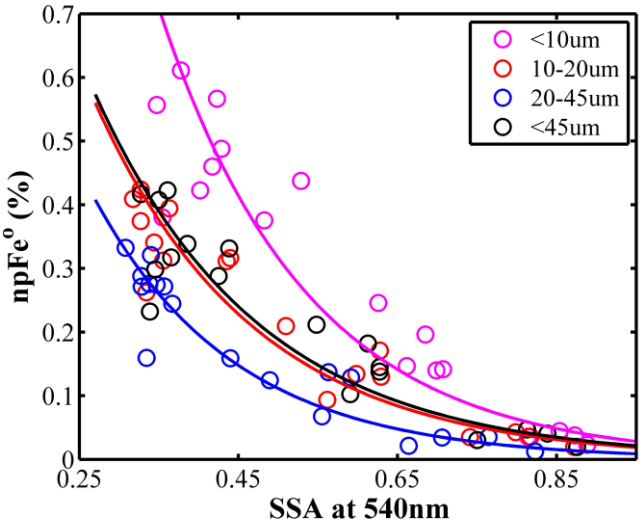

Figure 3. Correlation of SSA at 540 nm and npFe^0 for each grain size group of LSCC samples. Solid color lines represent regression lines for different size groups of lunar samples

Table 2. Model parameters and R^2 for each grain size group of LSCC data.

Grain Size	α	β	R^2
<10 μm	4.6478	5.375	0.90
10–20 μm	2.1549	4.991	0.92
20–45 μm	1.8737	5.648	0.89
<45 μm	2.1155	4.836	0.89

4.2. Correlation between the Ratio of 540 nm SSA/810 nm SSA and npFe^0

To minimize the effect of grain size, the correlation of the spectral ratio of 540 nm/810 nm SSA of all size groups of LSCC samples was calculated with npFe^0. It clearly reveals that a higher correlation was obtained with R^2 up to 0.91 (Figure 4) after normalizing 540 nm SSA by 810 nm SSA. Much less scattering is shown in Figure 4 than in Figure 3, which demonstrates the success of using the spectral ratio of 540 nm/810 nm SSA in minimizing the grain size effect. This pronounced improvement in npFe^0 estimation can be accounted for by several reasons. First, grain size has a significant influence on reflectance spectra at all wavelength regions [44,45,52]. By normalizing SSA at 540 nm to that at 810 nm, the effects of grain size could be significantly cancelled out. Second, both 540 nm and 810 nm are outside the absorption wavelength regions of lunar soils and cannot be largely affected by the Fe^{2+} absorption of lunar mafic minerals. Third, the ratio of 540 nm SSA over 810 nm SSA can be regarded as a slope measure for the reflected continuum at short spectral regions; the higher the npFe^0 included in a lunar soil is the redder the slope in the reflected continuum is, and vice versa.

Our result also suggests that this simple SSA ratio is suited for npFe^0 estimation of lunar soils showing a wide range of maturity (fresh, sub-mature, mature). Even for the mature lunar samples (I_s/FeO > 60), variation of npFe^0 can to some degree be reflected by the variation of the 540 nm/810 nm SSA ratio (Figure 5).

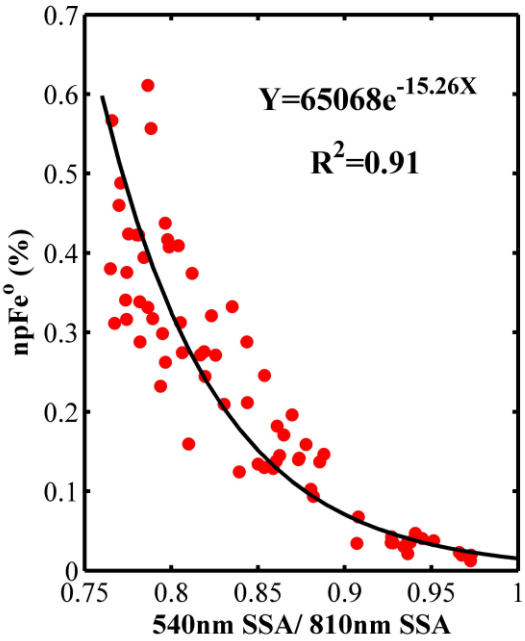

Figure 4. Correlation between the ratio of 540 nm SSA/810 nm SSA and $npFe^0$ for all size groups of LSCC soil samples.

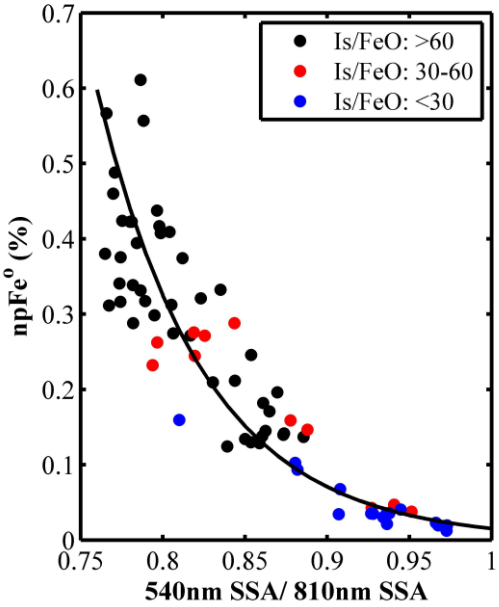

Figure 5. Correlation between the ratio of 540 nm SSA/810 nm SSA and $npFe^0$. Different solid color circles represent different maturity groups (I_s/FeO) of LSCC lunar samples. The black line is the regression line defined in Figure 4.

Although this empirical relationship was developed on the basis of LSCC data samples with a grain size < 45 μm, it might be also suited for estimating the $npFe^0$ of lunar soils with a larger grain size. Pieters et al. [1] measured the spectra of lunar soils as a function of grain size and found that while these lunar soils are extremely poorly sorted (varying from several microns to several hundred microns), the spectra of the bulk of the lunar soils were most similar to that of the finest size fraction (< 45 μm). The optical properties of lunar soils are dominated by this narrow size range because of their disproportionately large surface areas [1,53].

We also investigated the correlation between the $npFe^0$ and the ratio of 540 nm to 810 nm reflectance rather than SSA for all groups of LSCC samples (Figure 6). It can be seen that abundance of $npFe^0$ is poorly correlated with the ratio of 540 nm/810 nm reflectance of lunar soils. This is not unexpected because SSA is used to describe the scattering behavior of a single particle of lunar soil. $npFe^0$ in the amorphous rims of soil grains significantly influences a single particle's capability in reflecting or absorbing the incident light [10] and causes the SSA of lunar soils to be highly sensitive to the variation of $npFe^0$. However, in addition to SSA, the measured reflectance spectra of lunar soils are also influenced by other factors, such as multiple scattering and opposition effect [54], resulting in the unsensitivity of lunar soil spectra to the variation of $npFe^0$. Therefore, it is necessary to covert remotely obtained reflectance spectra to their corresponding SSA to estimate $npFe^0$ abundance in lunar soils.

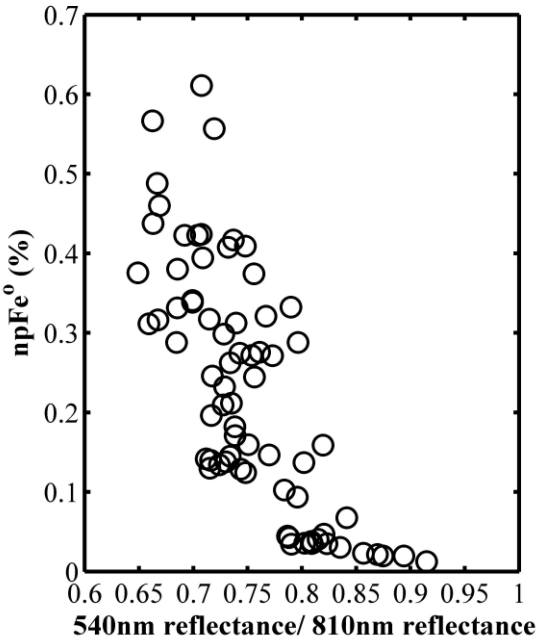

Figure 6. Correlation between the ratio of 540 nm reflectance/810 nm reflectance and $npFe^0$ for all size groups of LSCC soil samples.

5. Discussion

5.1. Scattering Points Analysis

Although normalizing 540 nm SSA by 810 nm SSA can partially remove the grain size effect of lunar soils and improve the correlation between $npFe^0$ abundance and the 540 nm/810 nm SSA ratio, there are still many points not tightly close to the regression line (Figure 4). This might be explained by two reasons. First, the scattering could result from the high ilmenite content of lunar soils. Trang and Lucey [38] attempted to derive $npFe^0$ abundance using Hapke's RTM and found that the variation of ilmenite content of lunar soils has a strong impact on the estimation result. This is consistent with our finding that many scattering points occur for soil samples with ilmenite content higher than 5% (Figure 7). The content of TiO_2, as the major composition of ilmenite, will increase in the soil samples with increasing ilmenite. Enhanced TiO_2 could result in a blue slope (in contrast to the reddening effect of $npFe^0$) of the reflectance spectra at short wavelengths [55,56]. Our regressed relationship as a measure of the slope for the reflectance continuum at short wavelengths could be affected by the enhanced TiO_2 content in lunar soils. We analyzed the correlation between $npFe^0$ and the 540 nm/810 nm SSA ratio for lunar samples of varying TiO_2 content. The result shows that some scattering points are samples with TiO_2 content higher than 6%. The correlation between $npFe^0$ abundance and the SSA ratio for lunar soils samples with TiO_2 content < 6% is remarkably better than (R^2 = 0.92) (Figure 8a) that for samples with TiO_2 content > 6% (R^2 = 0.11) (Figure 8b), indicating higher TiO_2 content within

lunar soils will to some extent interfere with the abundance prediction of $npFe^0$. Further correlation analysis on LSCC data suggests an obvious linear relationship between the ilmenite and TiO_2 content of lunar soils. 6% TiO_2 roughly corresponds to 5% ilmenite in lunar soils (Figure 9), which agrees well with our observation.

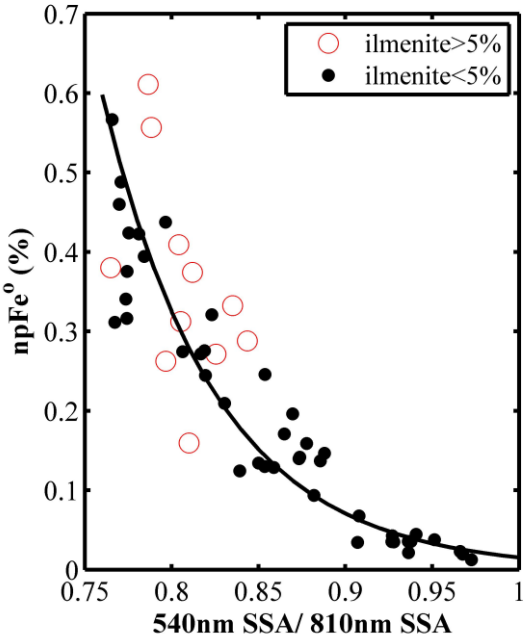

Figure 7. Correlation between the ratio of 540 nm SSA/810 nm SSA and $npFe^0$ denoted by different groups of LSCC lunar samples with varying ilmenite content. Solid black line is the regression line defined in Figure 4.

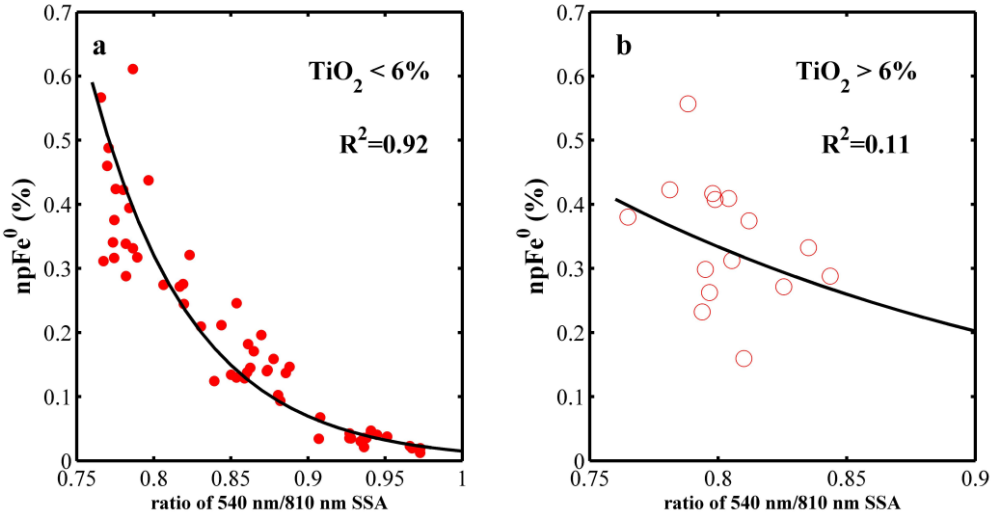

Figure 8. Correlation between the ratio of 540 nm SSA/810 nm SSA and $npFe^0$ for (**a**) lunar soil samples with TiO_2 content < 6% and for (**b**) lunar soil samples with TiO_2 content > 6%.

In addition to the interference from the ilmenite/TiO_2 content of lunar soils, some scattering points may result from samples possessing abundant (>55%) agglutinitic glass (Figure 10). Higher agglutinitic glass content in lunar soils could even cause the saturation of a regressed relationship in which the ratio of 540 nm/810 nm SSA changes very slightly with apparent increase in $npFe^0$ abundance (red circle in Figure 10). This is evidenced by the relatively higher correlation between the $npFe^0$ and SSA ratio for soil samples with agglutinitic glass < 55% (R^2 = 0.91) than that for soil samples with agglutinitic glass > 55% (R^2 = 0.78) (Figure 11). We attributed this result to the fact that in addition to the fine size $npFe^0$

coating on the surface of lunar soil grains, there are also large size metallic irons (>50 nm), termed as microphase iron or Britt-Pieters particle, residing in the interior of agglutinitic glass [38,57,58]. These larger size microphase irons mainly darken the lunar soils without much reddening effect compared to that of smaller size $npFe^0$ [58,59]. Higher abundance of large size microphase iron could accumulate in lunar soils as the agglutinitic glass content increases, resulting in a much flatter reflectance spectra of lunar soils at short wavelengths [46,49]. Therefore, the 510 nm/810 nm SSA ratio as a slope measure (reddening) at short wavelengths becomes insensitive to the variation of $npFe^0$ abundance.

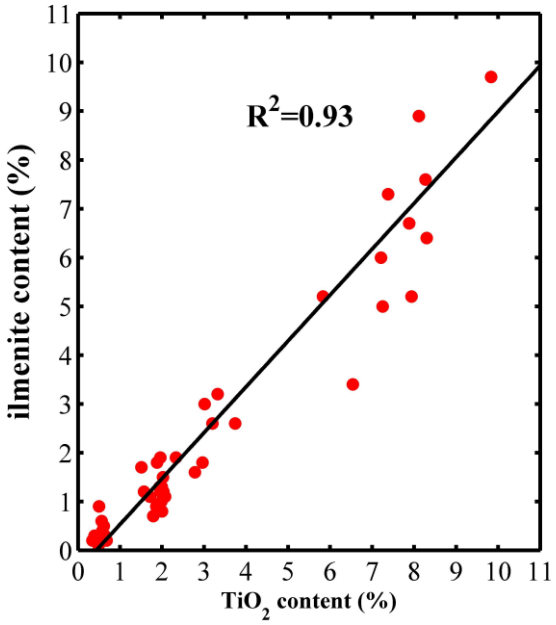

Figure 9. Linear correlation between ilmenite content and TiO_2 content of lunar soil samples.

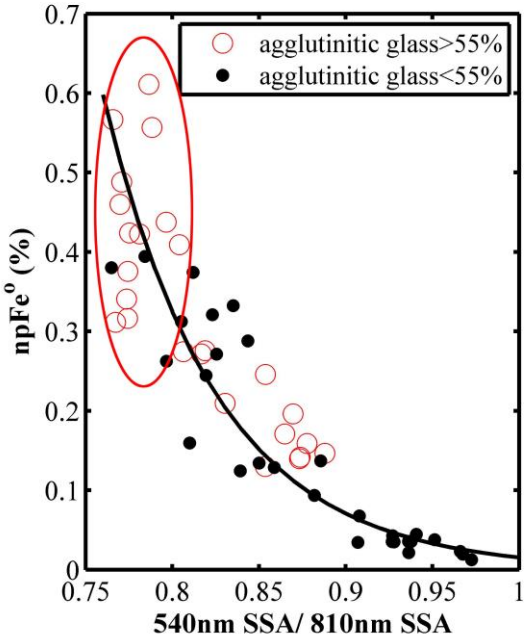

Figure 10. Correlation between the ratio of 540 nm SSA/810 nm SSA and $npFe^0$ denoted by different groups of LSCC lunar samples with varying agglutinitic glass content. Solid black line is the regression line defined in Figure 4.

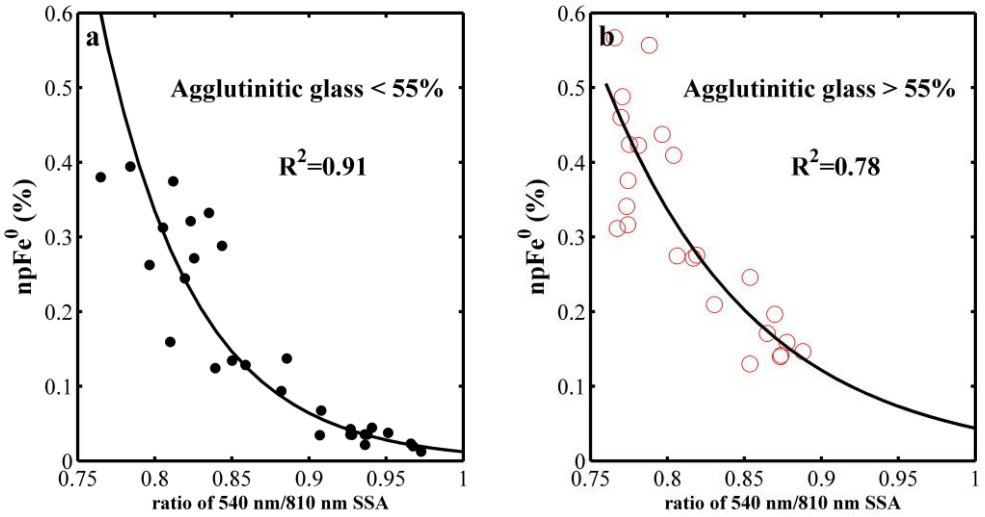

Figure 11. Correlation between the ratio of 540 nm SSA/810 nm SSA and $npFe^0$ for (**a**) lunar soil samples with agglutinitic glass content < 55% and for (**b**) lunar soil samples with agglutinitic glass content > 55%.

5.2. Non-linear Correlation Analysis

Figure 4 shows that the correlation between $npFe^0$ and the ratio of 540 nm SSA /810 nm SSA can be regressed using an exponential function rather than a linear function. One reason might be that higher agglutinitic glass content within lunar soils, as discussed in Section 5.1, could result in the unsensitivity of the 540 nm/ 810 nm SSA ratio to the variation of $npFe^0$ abundance. This can be demonstrated by the fact that a relatively acceptable linear relationship (R^2 = 0.82) exists between soil samples of lower agglutinitic glass content and $npFe^0$ abundance when soil samples of higher agglutinitic glass content were ignored (Figure 12a). Alternatively, it was found that if sub-mature soil samples were not considered, the correlation between $npFe^0$ and the ratio of 540 nm SSA/810 nm SSA can be also fitted by two separate linear functions corresponding to mature and fresh samples, respectively (Figure 12b). The exponential form seems to be the combination of these two linear forms. Mature soil samples show a steeper regressed slope and a lower R^2 compared to that of fresh soil samples. This is because the maturity of lunar soils roughly positively correlates with the their agglutinatuc glass content (Figure 13). Mature lunar soils might have an increased agglutinitic glass content relative to that of fresh soils. As discussed in 5.1, this could lead to the 540 nm/810 nm SSA changing very slightly with apparent variation in $npFe^0$ abundance. The two-segment linear fitting also implies that the maturity of lunar soils should be taken into account (e.g., optical maturity parameter: OMAT) in future work to further refine the model, and a linear correlation between $npFe^0$ abundance and the refined spectral parameter could be expected.

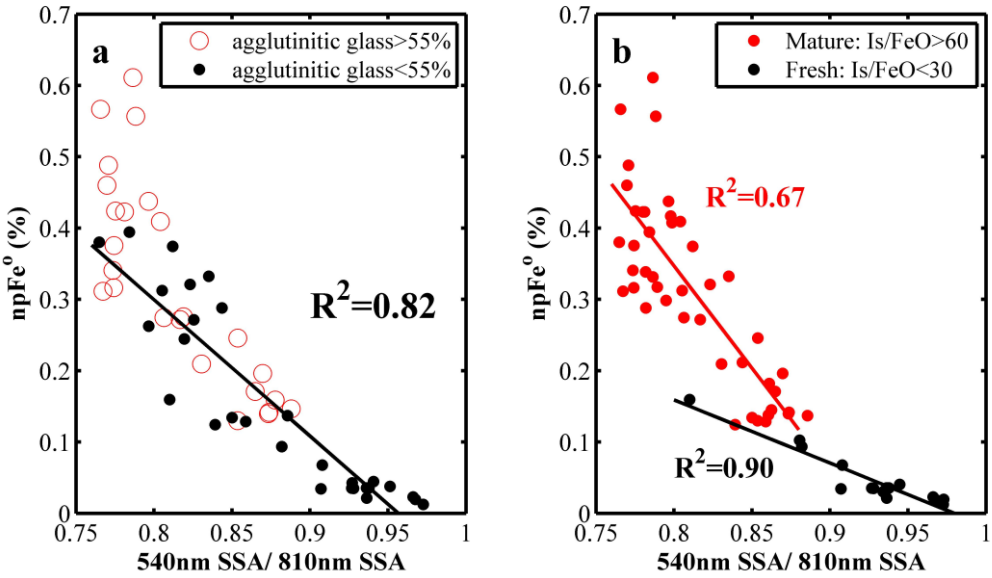

Figure 12. (**a**) Correlation between the ratio of 540 nm SSA/810 nm SSA and $npFe^0$ for lunar soil samples with agglutinitic glass content < 55%. Red circles are soil samples ignored in the regression process with agglutinitic glass content > 55%; (**b**) Correlation between the ratio of 540 nm SSA/810 nm SSA and $npFe^0$ for mature (red dots and line) and fresh (black dots and line) lunar soil samples.

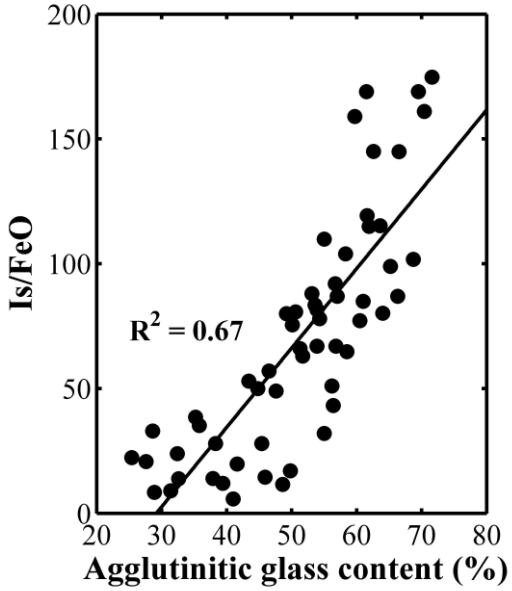

Figure 13. Correlation between the maturity (I_s/FeO) and agglutinitic glass content of LSCC lunar soil samples. Solid black line is the linear regression line.

5.3. Case Application and Comparison

Although accurate estimation of $npFe^0$ abundance in lunar soils based on the 540 nm /810 nm SSA ratio could be impeded by the agglutinitic glass and ilmenite content, this ratio can still be used to investigate the variation trend of $npFe^0$ for lunar surface areas. In this study, this empirical model was applied to a swirl and a mare region on the lunar surface to evaluate their regional $npFe^0$ distribution. The estimation results for the two regions were also compared, aiming at testing whether this model is sensitive to the variation of $npFe^0$ abundance in lunar soils.

1) Lunar swirls

Lunar swirls are bright curvilinear markings on the lunar surface. They are optically immature compared to the surrounding areas and associated with regions having high magnetic field strength [60,61]. One prevailing hypothesis for the origin of lunar swirls states that the magnetic field above swirl surfaces deflects the solar wind ions away from swirl regions and directs them to the off-swirl regions. Less $npFe^0$ is generated in swirl regions than surrounding off-swirl regions owing to reduced solar wind flux [62,63]. This provides the best target area for our model evaluation.

We applied the model (exponential function in Figure 4) to one sub-image of M^3 level 2 reflected spectral data covering the central region of a famous lunar swirl 'Reiner Gamma' (Figure 14a) to assess whether the mapped $npFe^0$ distribution geographically agrees well with the bright swirl observed in the remote sensing image.

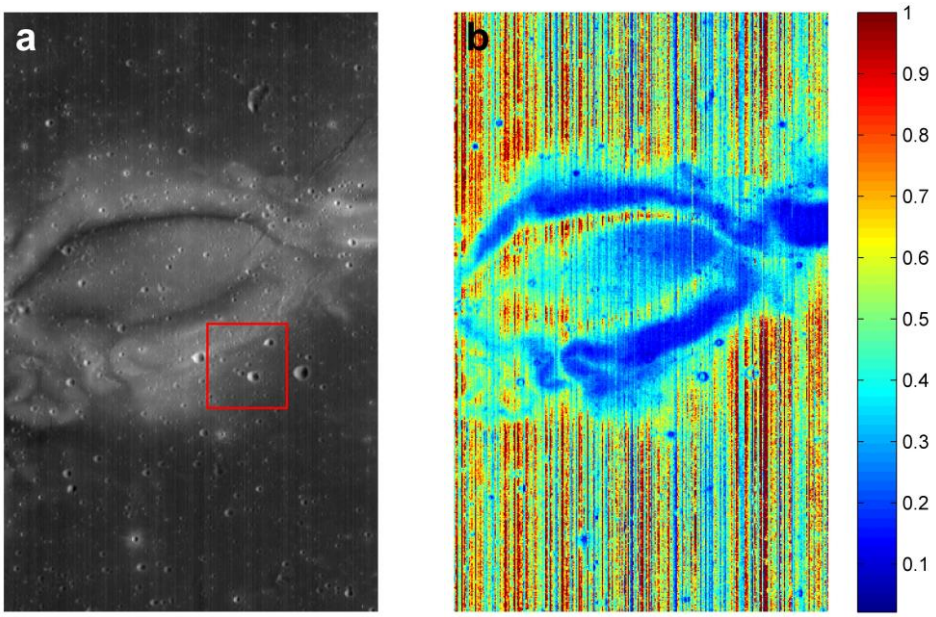

Figure 14. (**a**) M^3 750 nm reflectance image for lunar swirl 'Reiner Gamma'; (**b**) $npFe^0$ abundance distribution of 'Reiner Gamma'.

Our results show that the swirl region evidently possesses a lower amount of $npFe^0$ relative to the off-swirl region (Figure 14b). The bright swirl in the image (Figure 14a) geographically correlates well with the lunar surface of decreased $npFe^0$, and the outline of swirl can be fully characterized by the areas deficient in $npFe^0$ abundance.

The geographical agreement between the 750 nm reflectance image and $npFe^0$ distribution map is reasonable and not an artifact resulting from higher correlation between reflectance data and their corresponding SSA. Although reflectance at 750 nm correlates with the single band SSA at 540 nm or 810 nm to some degree, it is not necessarily correlated with the ratio of 540 nm SSA/810 nm SSA. Shown in Figure 15a,b are the reflectance image at 750 nm of one sub-area in Figure 14a (red square) and the ratio image of 540 nm SSA/810 nm SSA of that sub-area, respectively. It can be seen that although some areas are positively correlated (bright area indicated by red arrows), other surface areas are negatively correlated. Parts of crater walls or floors (yellow arrow) with higher reflectance at 750 nm show a decreased ratio of 540 nm SSA/810 nm SSA, contrasting to the trend seen in the bright areas (red arrow). Some small craters in the 750 nm reflectance image (Figure 15a) even disappear in the SSA ratio image (Figure 15b) (green arrow). These observations suggest that the geographical correlation between derived $npFe^0$ distribution and 750 nm reflectance is not an artifact of the way the data reduced. Single band reflectance (e.g., 750 nm reflectance) reflects the brightness variation of the lunar surface, and it can be influenced by many factors such as variation in grain size and composing minerals of lunar soils, shadow effects, topography variation and viewing geometry. Using one band

reflectance or SSA alone cannot provide a reliable prediction of $npFe^0$ abundance (Figure 2). However, the ratio of 540 nm SSA/810 nm SSA can partially remove these effects, amplifying the $npFe^0$ effect on regulating the short wavelength spectra (Figure 4). It is capable of reflecting the regional $npFe^0$ variation trend when there is indeed $npFe^0$ abundance difference within lunar soils. The effectiveness of this ratio in $npFe^0$ estimation can also be validated by the fact that the derived abundance of $npFe^0$ within this region ranges from 0% to 1% close to the reported values of lunar soil samples [41] and the predicted values from remote sensing data [38].

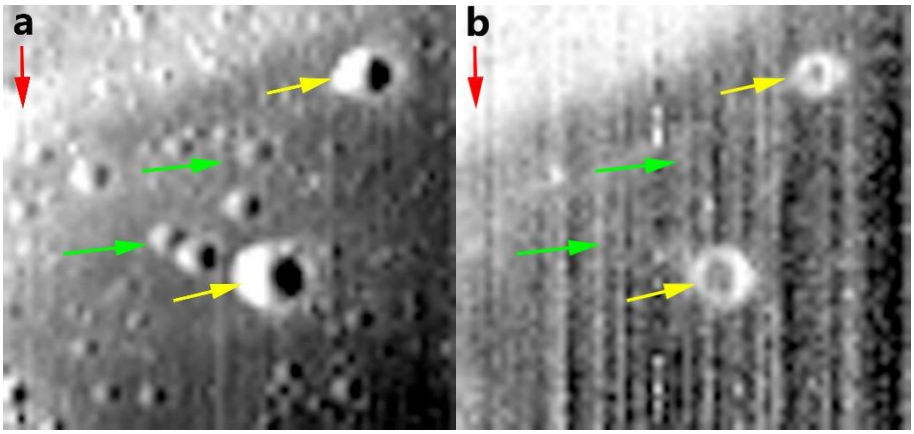

Figure 15. (**a**) M^3 750 nm reflectance image of one sub-area in Figure 14a (red box); (**b**) the ratio of 540 nm/810 nm SSA of this sub-area. Red arrow shows positively correlated bright swirl regions between the two images. Yellow arrows show some parts of crater wall or floor having higher brightness in the 750 nm reflectance image while having low values in the 540 nm/810 nm SSA ratio image. Green arrows show the craters disappeared in the 540 nm/810 nm SSA ratio image.

2) Lunar maria

To make a comparison with the swirl region, distribution of $npFe^0$ of a mare region to the north of 'Reiner Gamma' was also investigated. This mare region is relative homogenous without apparent albedo difference across its surface, except some distributed fresh impact craters (Figure 16a). It is expected that the $npFe^0$ variation for this region should not be as strong as that of the lunar swirl (Figure 14b).

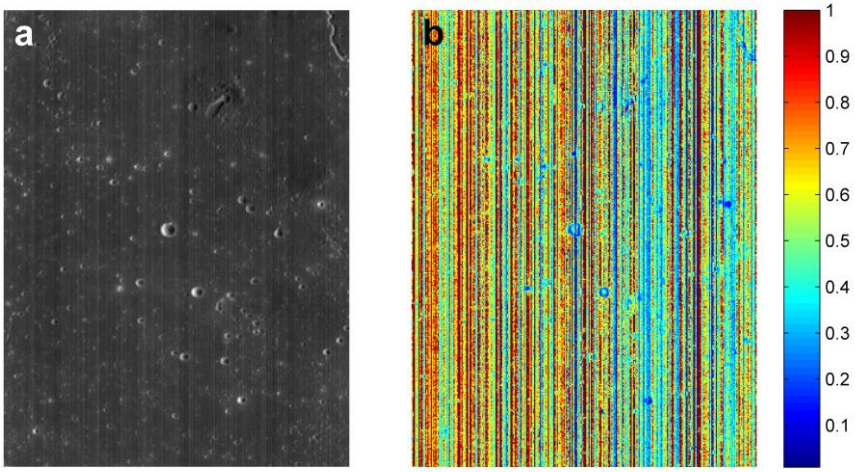

Figure 16. (**a**) M^3 750 nm reflectance image of the mare region to the north of Reiner Gamma; (**b**) $npFe^0$ abundance distribution.

By applying this empirical model to this mare region, it was found that, in contrast to the large $npFe^0$ abundance difference between the swirl and off-swirl regions in Figure 14b, no surface area with obvious decreased or increased $npFe^0$ can be observed within this mare region (Figure 16b). The $npFe^0$ distribution of the whole region only bears resemblance to that of the off-swirl regions in Figure 14b.

It is worth noting that even in such areas without significant $npFe^0$ variation, the fresh craters on the surface of the mare can still be clearly revealed by regional distribution of $npFe^0$ (blue round spots or rings in Figure 16b). These fresh craters show a decreased amount of $npFe^0$ consistent with what is expected on the lunar surface. Because of the short exposure time to a space weathering environment, a lower amount of $npFe^0$ could have accumulated in these craters relative to the surrounding lunar soils [43]. This also demonstrates the effectiveness of this empirical model in estimating $npFe^0$ abundance of the lunar surface. However, many strips can be seen in both investigated swirl and mare regions (Figures 14b and 16b). This can be ascribed to the noise originating in the original M^3 data (strips in Figures 14a and 16a) rather than a true variation of $npFe^0$ abundance.

6. Conclusions

The 540 nm/810 nm SSA ratio is highly correlated to $npFe^0$ abundance in lunar soils. This spectral ratio highlights the spectral importance of $npFe^0$, reduces the grain size effect of lunar soils on the short wavelengths reflectance spectra and, thus, can be considered as a useful spectral index for the prediction of $npFe^0$ abundance within lunar soils.

However, the performance of this simple empirical model does show some interference from the high content of agglutinitic glass and ilmenite in lunar soils. More work regarding removing the effects of high agglutitinic glass and ilmenite/TiO_2 content should be considered in future work to further refine the model's performance in estimating $npFe^0$ abundance of lunar soils.

Author Contributions: Data curation, B.L. and R.X.; Formal analysis, D.L.; Investigation, G.Z.; Methodology, D.L.; Project administration, C.L.; Resources, B.L.; Validation, X.R. and C.L.; Writing—original draft preparation, D.L.; writing—review and editing, Y.Z. All authors have read and agreed to the published version of the manuscript.

Funding: This work was supported by the National Natural Science Foundation of China (41601374, 11941002 and 61605231) and by the B-type Strategic Priority Program of the Chinese Academy of Sciences (XDB41000000).

Acknowledgments: We thank Kevin Cannon and an anonymous reviewer for their constructive reviews and comments, which greatly improved this manuscript. We also thank the Reflectance Experiment Laboratory (Relab) of Brown University and Planetary Geoscience Institute of the University of Tennessee for making the LSCC dataset publicly available.

Conflicts of Interest: The authors declare no conflicts of interest.

Appendix A

An approximate solution to the radiative transfer equations was proposed by [10,54,64] to describe the light scattering behavior of lunar soils based on the assumption that lunar surface materials are intimately mixed and lunar soil grains are closely spaced with their size larger than spectral wavelengths. In his work, the reflectance spectra of lunar soils can be converted to its SSA by the following equation:

$$R = \frac{\omega}{4}\frac{1}{\mu_0 + \mu}\{[1 + B(g)] \times P(g) + H(\mu_0, \omega) \times H(\mu, \omega) - 1\} \quad (A1)$$

Here, R is remotely obtained or lab-measured reflectance, ω is the SSA of lunar soils, μ_0 and μ are the cosine of the incidence light angle (i) and emittance light angle (e), respectively. g is the phase angle. B(g) and P(g) are the backscattering function and phase function of lunar soils, and H represents the multiple scattering effect between lunar soil grains.

It was found that the backscattering function B(g) defining the opposition effect of lunar soils decreases significantly with increasing phase angle g and can be ignored when g is greater than 15° [54]. Because all the reflectance spectra of the soil samples used in this study were measured at phase angle

30° and most of the remotely obtained reflectance spectra such as M^3 data had also been photometrically corrected to the phase angle 30°, B(g) was set to be zero to ignore the backscattering effect of lunar soils. To further simplify the model, the lunar soils were considered as isotropic scattering and the phase function P(g) was set to be unity in this study. This assumption was adopted and supported by the work [65], which found that it will not strongly affect the performance of Hapke's RTM. According to these assumptions, Equation (A1) can be simplified as follows:

$$R = (\omega \times H(\mu_0, \omega) \times H(\mu, \omega)) / (4 \times (\mu + \mu_0)) \quad (A2)$$

Here, $H(x, \omega)$ is Chanderasekhar's function for isotropic scattering of lunar soils, and x represents μ_0 (incident light angle) or μ (emittance light angle) [50].

Setting the incidence angle and emission angle as 30° and 0°, the same as the measured reflectance data of lunar soil samples in this study, the SSA of lunar soils could be derived from Equation (A1) and Equation (A2) as follows [50]:

$$\omega = 1 - \left(\frac{-27.865R + \sqrt{4.029R^2 + 602.932R + 268.696}}{51.71R + 16.392} \right)^2 \quad (A3)$$

These steps are the same as the work of Yan et al. [50].

References

1. Pieters, C.M.; Fischer, E.M.; Rode, O.; Basu, A. Optical effects of space weathering-the role of the finest fraction. *J. Geophys. Res.* **1993**, *98*, 20817–20824. [CrossRef]
2. Chapman, C.R. Space weathering of asteroid surfaces. *Annu. Rev. Earth Planet. Sci.* **2004**, *32*, 539–567. [CrossRef]
3. Hapke, B. Interpretations of optical observations of Mercury and the moon. *Phys. Earth Planet. Interi.* **1977**, *15*, 264–274. [CrossRef]
4. Hapke, B.; Cohen, A.; Cassidy, W.; Wells, E. Solar radiation effects on the optical properties of Apollo 11 lunar samples. In Proceedings of the Apollo 11 Lunar Science Conference, Houston, TX, USA, 5–8 January 1970; pp. 2199–2212.
5. Noble, S.K.; Pieters, C.M. Space weathering on Mercury: Implications for remote sensing. *Sol. Syst. Res.* **2003**, *37*, 31–35. [CrossRef]
6. Brunetto, R.; Vernazza, P.; Marchi, S.; Birlan, M.; Fulchignoni, M.; Orofino, V.; Strazzulla, G. Modeling asteroid surfaces from observations and irradiation experiments: The case of 832 Karin. *Icarus* **2006**, *184*, 327–337. [CrossRef]
7. Pieters, C.M.; Taylor, L.A.; Noble, S.K.; Keller, L.P.; Hapke, B.; Morris, R.V.; Allen, C.C.; McKay, D.S.; Wentworth, S. Space weathering on airless bodies: Resolving a mystery with lunar samples. *Meteorit. Planet. Sci.* **2000**, *35*, 1101–1107. [CrossRef]
8. McCord, T.B.; Johnson, T.V. Lunar spectral reflectivity (0.30 to 2.50 microns) and implications for remote mineralogical analysis. *Science* **1970**, *169*, 855–858. [CrossRef]
9. McCord, T.B.; Adams, J.B. Progress in remote optical analysis of lunar surface composition. *Moon* **1973**, *7*, 453–474. [CrossRef]
10. Hapke, B. Space weathering from Mercury to the asteroid belt. *J. Geophys. Res.* **2001**, *106*, 10039–10073. [CrossRef]
11. Conel, J.; Nash, D. Spectral reflectance and albedo of Apollo 11 lunar samples: Effects of irradiation and vitrification and comparison with telescopic observations. *Geochim. Cosmochim. Acta* **1970**, *1*, 2013–2024.
12. Cassidy, W.; Hapke, B. Effects of darkening processes on surfaces of airless bodies. *Icarus* **1975**, *25*, 371–383. [CrossRef]
13. Keller, L.P.; Mckay, D.S. Discovery of vapor deposits in the Lunar Regolith. *Science* **1993**, *261*, 1305–1307. [CrossRef] [PubMed]
14. Keller, L.P.; McKay, D.S. The nature and origin of rims on lunar soil grains. *Geochim. Cosmochim. Acta* **1997**, *61*, 2331–2341. [CrossRef]

15. Taylor, L.A.; Pieters, C.M.; Keller, L.P.; Morris, R.V.; McKay, D.S. Lunar mare soils: Space weathering and the major effects of surface-correlated nanophase Fe. *J. Geophys. Res.* **2001**, *106*, 27985–27999. [CrossRef]
16. Taylor, L.A.; Pieters, C.M.; Patchen, A.; Taylor, D.S.; Morris, R.V.; Keller, L.P.; Mckay, D.S. Mineralogical and chemical characterization of lunar highland soils: Insights into the space weathering of soils on airless bodies. *J. Geophys. Res.* **2010**, *115*, E02002. [CrossRef]
17. Hapke, B. Effects of a simulated solar wind on the photometric properties of rocks and powders. *Ann. N. Y. Acad. Sci.* **1965**, *123*, 711–721. [CrossRef]
18. Stern, A. The lunar atmosphere: History, status, current problems, and context. *Rev. Geophys.* **1999**, *37*, 453–491. [CrossRef]
19. Crider, D.H.; Vondrak, R.R. Hydrogen migration to the lunar poles by solar wind bombardment of the moon. *Adv. Space Res.* **2002**, *30*, 1869–1874. [CrossRef]
20. Housley, R.M. A model for chemical and isotopic fractionation in the lunar regolith by impact vaporization. In Proceedings of the Lunar and Planetary Science Conference, Houston, TX, USA, 19–23 March 1979.
21. Thompson, M.S.; Zega, T.J.; Howe, J.Y. In Situ experimental formation and growth of Fe nanoparticles and vesicles in lunar soil. *Meteoritics Planet. Sci.* **2017**, *52*, 413–427. [CrossRef]
22. Dukes, C.; Baragiola, R.; McFadden, L. Surface modification of olivine by H^+ and He^+ bombardment. *J. Geophys. Res. Planets* **1999**, *104*, 1865–1872. [CrossRef]
23. Loeffler, M.; Dukes, C.; Baragiola, R. Irradiation of olivine by 4 keV He^+: Simulation of space weathering by the solar wind. *J. Geophys. Res. Planets* **2009**, *114*, E03003. [CrossRef]
24. Christoffersen, R.; Rahman, Z.; Keller, L. Solar ion sputter deposition in the lunar regolith: Experimental simulation using focused-ion beam techniques. In Proceedings of the Lunar and Planetary Science Conference, The Woodland, TX, USA, 19–23 March 2012; p. 2614.
25. Sasaki, S.; Nakamura, K.; Hamabe, Y.; Kurahashi, E.; Hiroi, T. Production of iron nanoparticles by laser irradiation in a simulation of lunar-like space weathering. *Nature* **2001**, *410*, 555–557. [CrossRef] [PubMed]
26. Sasaki, S.; Hiroi, T.; Nakamura, K.; Hamabe, Y.; Kurahashi, E.; Yamada, M. Simulation of space weathering by nanosecond pulse laser heating: Dependence on mineral composition, weathering trend of asteroids and discovery of nanophase iron particles. *Adv. Sp. Res.* **2002**, *29*, 783–788. [CrossRef]
27. Gillis-Davis, J.; Gasda, P.; Bradley, J.; Ishii, H.; Bussey, D. Laser space weathering of Allende (CV2) and Murchison (CM2) carbonaceous chondrites. In Proceedings of the Lunar and Planetary Science Conference, The Woodlands, TX, USA, 16–20 March 2015; p. 1607.
28. Matsuoka, M.; Nakamura, T.; Kimura, Y.; Hiroi, T.; Nakamura, R.; Okumura, S.; Sasaki, S. Pulse-laser irradiation experiments of Murchison CM2 chondrite for reproducing space weathering on C-type asteroids. *Icarus* **2015**, *254*, 135–143. [CrossRef]
29. Thompson, M.S.; Zega, T.J.; Becerra, P.; Keane, J.T.; Byrne, S. The oxidation state of nanophase fe particles in lunar soil: Implications for space weathering. *Meteorit. Planet. Sci.* **2016**, *51*, 1082–1095. [CrossRef]
30. Housley, R.M.; Grant, R.W.; Paton, N.E. Origin and characteristics of excess Fe metal in lunar glass welded aggregates. In Proceedings of the Lunar Science Conference, Houston, TX, USA, 5–8 March 1973; pp. 2737–2749.
31. Bandfield, J.L.; Poston, M.J.; Klima, R.L.; Edwards, C.S. Widespread distribution of OH/H2O on the lunar surface inferred from spectral data. *Nat. Geosci.* **2018**, *11*, 173–177. [CrossRef]
32. Hood, L.L.; Schubert, G. Lunar magnetic anomalies and surface optical properties. *Science* **1980**, *208*, 49–51. [CrossRef]
33. Hood, L.L.; Williams, C.R. The lunar swirls: Distribution and possible origins. In Proceedings of the Lunar and Planetary Science Conference, Houston, TX, USA, 14–18 March 1989; pp. 99–113.
34. Blewett, D.T.; Coman, E.I.; Hawke, B.R.; Gillis-Davis, J.J.; Purucker, M.E.; Hughes, C.G. Lunar swirls: Examining crustal magnetic anomalies and space weathering trends. *J. Geophys. Res.* **2011**, *116*, E02002.
35. Hiroi, T.; Pieters, C.M.; Morris, R.V. New Considerations for estimating lunar soil maturity from VIS-NIR reflectance spectroscopy. In Proceedings of the Lunar and Planetary Science Conference, Houston, TX, USA, 16–20 March 1998; p. 1152.
36. Mouélic, S.L.; Langevin, Y.; Erard, S. Discrimination between maturity and composition of lunar soils from integrated Clementine UV-visible/near-infrared data: Application to the Aristarchus Plateau. *J. Geophys. Res.* **2000**, *105*, 9445–9455. [CrossRef]

37. Pieters, C.; Shkuratov, Y.; Kaydash, V.; Stankevich, D.; Taylor, L. Lunar soil characterization consortium analyses: Pyroxene and maturity estimates derived from Clementine image data. *Icarus* **2006**, *184*, 83–101. [CrossRef]
38. Trang, D.; Lucey, P.G. Improved space weathering maps of the lunar surface through radiative transfer modeling of Kaguya multiband imager data. *Icarus* **2019**, *321*, 307–323. [CrossRef]
39. Morris, R.V. Surface exposure indices of lunar rocks: A comparative FMR study. In Proceedings of the Lunar and Planetary Science Conference, Houston, TX, USA, 15–19 March 1976; pp. 315–335.
40. Morris, R.V. The surface exposure (maturity) of lunar soils: Some concepts and Is/FeO compilation. In Proceedings of the Lunar and Planetary Science Conference, Houston, TX, USA, 13–17 March 1978; pp. 2278–2297.
41. Morris, R.V. Origins and size distribution of metallic iron particles in the lunar regolith. In Proceedings of the Lunar and Planetary Science Conference, Houston, TX, USA, 17–21 March 1980; pp. 1697–1712.
42. Heiken, G.; McKay, D.S. Petrography of Apollo 17 soils. In Proceedings of the Lunar and Planetary Science Conference, Houston, TX, USA, 18–22 March 1974; pp. 843–860.
43. Noble, S.K.; Pieters, C.M.; Taylor, L.A.; Morris, R.V.; Allen, C.C.; McKay, D.S.; Keller, L.P. The optical properties of the finest fraction of lunar soil: Implications for space weathering. *Meteorit. Planet. Sci.* **2001**, *36*, 31–42. [CrossRef]
44. Liu, D.; Li, L.; Zhang, Y.Z. Sensitivity analysis for Hapke's radiative transfer model. In Proceedings of the Lunar and Planetary Science Conference, The Woodlands, TX, USA, 18–22 March 2013; p. 1290.
45. Liu, D. Improvement and Use of Radiative Transfer Models to Assess Lunar Space Weathering and Mechanisms for Swirl Formation. Ph.D. Thesis, Indiana University, Indiana, IN, USA, 2015.
46. Noble, S.K.; Pieters, C.M.; Keller, L.P. An experimental approach to understanding the optical effects of space weathering. *Icarus* **2007**, *192*, 629–642. [CrossRef]
47. Fischer, E.M.; Pieters, C.M.; Pratt, S.F. Modeling the space weathering-induced optical alteration of lunar soils: First results. In Proceedings of the Lunar and Planetary Science Conference, Houston, TX, USA, 15–19 March 1994; pp. 371–372.
48. Fischer E., M.; Pieters, C.M. A Model for lunar soil optical alteration due to space weathering. In Proceedings of the Lunar and Planetary Science Conference, Houston, TX, USA, 14–18 March 1995; pp. 395–396.
49. Wohlfarth, K.S.; Wöhler, C.; Grumpe, A. Space Weathering and Lunar OH/H_2O—Insights from Ab Initio Mie Modeling of Submicroscopic Iron. *Astron. J.* **2019**, *158*, 80. [CrossRef]
50. Yan, B.; Wang, R.; Gan, F.; Wang, Z. Minerals mapping of the lunar surface with Clementine UVVIS/NIR data based on spectra unmixing method and Hapke model. *Icarus* **2010**, *208*, 11–19. [CrossRef]
51. Adams, J.B.; Filice, A.L. Spectral reflectance 0.4 to 2.0 microns of silicate rock powders. *J. Geophys. Res.* **1967**, *72*, 5705–5715. [CrossRef]
52. Pieters, C.M. Strength of mineral absorption features in the transmitted component of near-infrared reflected light: First results from RELAB. *J. Geophys. Res.* **1983**, *88*, 9534–9544. [CrossRef]
53. Lucey, P.G. Radiative transfer modeling of the effect of mineralogy on some empirical methods for estimating iron concentration from multispectral imaging of the Moon. *J. Geophys. Res.* **2006**, *111*, E08003. [CrossRef]
54. Hapke, B. Bidirectional reflectance spectroscopy: 1. Theory. *J. Geophys. Res.* **1981**, *86*, 3039–3054. [CrossRef]
55. Lucey, P.G.; Blewett, D.T.; Hawke, B.R. Mapping the FeO and TiO_2 content of the lunar surface with multispectral inagery. *J. Geophys. Res.* **1998**, *103*, 3679–3699. [CrossRef]
56. Johnson, J.R.; Larson, S.M.; Singer, R.B. Remote sensing of potential lunar resources: 1. Near-Side compositional properties. *J. Geophys. Res.* **1991**, *96*, 18861–18882. [CrossRef]
57. Pieters, C.M.; Noble, S.K. Space weathering on airless bodies. *J. Geophys. Res.* **2016**, *121*, 1865–1884. [CrossRef] [PubMed]
58. Lucey, P.G.; Riner, M.A. The optical effects of small iron particles that darken but do not redden: Evidence of intense space weathering on Mercury. *Icarus* **2011**, *212*, 451–462. [CrossRef]
59. Liu, D.; Li, L.; Sun, Y. An improved radiative transfer model for estimating mineral abundance of immature and mature lunar soils. *Icarus* **2015**, *253*, 40–50. [CrossRef]
60. Schultz, P.H.; Srnka, L.J. Cometary collisions on the Moon and Mercury. *Nature* **1980**, *284*, 22–26. [CrossRef]
61. Richmond, N.C.; Hood, L.L.; Mitchell, D.L.; Lin, R.P.; Acuna, M.H.; Binder, A.B. Correlations between magnetic anomalies and surface geology antipodal to lunar impact basins. *J. Geophys. Res.* **2005**, *110*, E05011. [CrossRef]

62. Besse, S.; Dhingra, D.; Nettles, J.; Klima, R.; Garrick-Bethell, I.; Clark, R.N.; Combe, J.P.; Head, J.W., III; Taylor, L.A.; Pieters, C.M.; et al. M^3 spectral analysis of lunar swirls and the link between optical maturation and surface hydroxyl formation at magnetic anomalies. *J. Geophys. Res.* **2011**, *116*, E9.
63. Kramer, G.Y.; Combe, J.P.; Harnett, E.M.; Hawke, B.R.; Noble, S.K.; Blewett, D.T.; McCord, T.B.; Giguere, T.A. Characterization of lunar swirls at Mare Ingenii: A model for space weathering at magnetic anomalies. *J. Geophys. Res. Planet* **2011**, *16*, E04008. [CrossRef]
64. Hapke, B. *Theory of Reflectance and Emittance Spectroscopy*; Cambridge University Press: New York, NY, USA, 2005.
65. Mustard, J.F.; Pieters, C.M. Photometric phase functions of common geologic minerals and applications to quantitative analysis of mineral mixture reflectance spectra. *J. Geophys. Res. Solid Earth* **1989**, *94*, 13619–13634. [CrossRef]